Cement and Concrete Research 40 (2010) 1531–1540

Contents lists available at ScienceDirect

Cement and Concrete Research

journal homepage: http://ees.elsevier.com/CEMCON/default.asp

# Analytical solutions for bleeding of concrete due to consolidation

P.H. Morris *, P.F. Dux

*School of Civil Engineering, University of Queensland, Brisbane, Queensland 4072, Australia*

ARTICLE INFO

*Article history:*
Received 30 July 2007
Accepted 21 June 2010

*Keywords:*
Bleeding (A)
Fresh concrete (A)
Hydration (A)
Modelling (E)
Analytical solutions

ABSTRACT

The bleeding of cement pastes, cement mortars, and concrete is due primarily to the self-weight consolidation of the granular skeleton formed by the solid constituents thereof. However, the effects of hydration can end this process prematurely. Linear finite- and small-strain analytical solutions of bleeding as a consolidation process that account for the effects of hydration are presented and then validated by comparison with laboratory data for cement pastes and concretes. Contrary to earlier assertions that a finite-strain model is required to model bleeding, the new finite- and small-strain solutions model the bleeding of the relatively shallow specimens analysed equally well. However, further research is necessary to establish whether small-strain solutions can model adequately the bleeding of comparatively deep concrete layers, and methods of determining the values of input parameters for the new solutions are also required. A potential method of determining one of these, the time of set, is discussed briefly.



## 1. Introduction

The significance of the bleeding of cement pastes, cement mortars, and concretes, which has a major impact on plastic cracking, and the importance of understanding it have long been recognised [1,2]. Bleeding has consequently been the subject of considerable research efforts spanning many years and remains so today [3–5]. In particular, analyses of bleeding as a process of self-weight consolidation have been presented by a number of researchers [1,4–7] over a very long period.

The earliest such analysis is that of Powers [1], who concluded that bleeding was attributable to a process of subsidence that eventually halted either because mechanical consolidation was complete or because of the beginning of set. Powers presented a small-strain consolidation theory that accounts for hydration but gave a numerical solution only.

Considerably later, Tan et al. [6] derived a small-strain analytical solution of the bleeding of cement pastes that neglects hydration and can be shown to be identical to an earlier solution for the consolidation of soil [8]. Their comparison of the solution with laboratory data [6] indicated that it would be necessary to account for hydration to obtain satisfactory fits. Kwak and Ha [4] subsequently validated the small-strain model using earlier data for cement pastes and concretes, and Tan et al. [7] presented a finite-strain model of the bleeding of cement pastes and mortars that considered the effect of set. The latter was solved numerically and validated by comparison with data for cement pastes and mortars [7].

Most recently, Kwak and Ha [4] presented a small-strain numerical model of bleeding that accounts for the temperature variation caused by the heat of hydration, but not for set, while Josserand et al. [5] presented a finite-strain numerical model that incorporates the effects of hydration.

In this paper, linear finite-strain and small-strain analytical solutions for the bleeding of fresh cement pastes, cement mortars, and concretes due to one-dimensional self-weight consolidation are presented that account for set. The effects of temperature changes, including those due to the heat of hydration, are ignored. The solutions are validated by comparison with laboratory data for cement pastes and concretes taken from the literature, and their potential applications and limitations are discussed. A potential method of determining the time of set, an important parameter in the analytical solutions, is also discussed briefly.

## 2. Analytical solutions of self-weight consolidation

The presence of entrained air, which typically occupies about 1% to 5% of the volume of plastic concrete, is neglected in earlier self-weight consolidation models for the bleeding of cement paste, cement mortar, and concrete [5–7] and in comparable models of the consolidation of soils [8,9]. It is also neglected in the models presented here.

In the following derivations, the material as a whole and the liquid in the pores, are, for convenience, referred to as concrete and water, respectively, regardless of their composition. The term, concrete, thus includes cement pastes and cement mortars.

* Corresponding author. Tel.: +61 7 3365 3518; fax: +61 7 3365 4599.
*E-mail address:* p.morris@uq.edu.au (P.H. Morris).

0008-8846/$ – see front matter © 2010 Elsevier Ltd. All rights reserved.
doi:10.1016/j.cemconres.2010.06.007

### 2.1. Governing equations

The governing equation in material co-ordinates for one-dimensional primary consolidation (neglecting creep) of a saturated, thick concrete layer is [10]

$$-\left(\frac{\gamma_s}{\gamma_w}-1\right)\frac{d}{de}\left(\frac{k(e)}{(1+e)}\right)\frac{\partial e}{\partial z}+\frac{\partial}{\partial z}\left(\frac{k(e)}{\gamma_w(1+e)}\frac{d\sigma'}{de}\frac{\partial e}{\partial z}\right)+\frac{\partial e}{\partial t}=0 \tag{1}$$

where $\gamma_s$ is the unit weight of the solids, $\gamma_w$ the unit weight of water, $e$ the void ratio, $k$ the vertical permeability, $z$ the vertical material co-ordinate measured downwards from the top of the concrete, $t$ the time measured from the end of placing, and $\sigma'$ the vertical effective stress.

Natural and material co-ordinates are related by [8,10,11]

$$z=\int_0^x\frac{1}{(1+e_i(x))}dx \tag{2}$$

where $x$ is the natural vertical co-ordinate measured downwards from the top of the concrete and $e_i(x)$ is the $e$ at zero $t$.

Eq. (1) was introduced by Gibson et al. [10] to overcome the shortcomings of the small-strain Terzaghi solution [9]. The small-strain governing equation, expressed in material co-ordinates, is [12]

$$\frac{\partial^2 e}{\partial z^2}=\frac{1}{g}\frac{\partial e}{\partial t} \tag{3}$$

where $g$ is the finite-strain coefficient of consolidation.

The parameter $g$ is related to the classical Terzaghi small-strain coefficient of consolidation $c_v$ by [12,13]

$$g=\frac{c_v}{(1+e)^2} \tag{4}$$

Gibson et al. [13] reduced Eq. (1) to the linear form

$$\frac{\partial^2 e}{\partial z^2}+\lambda(\gamma_s-\gamma_w)\frac{\partial e}{\partial z}=\frac{1}{g}\frac{\partial e}{\partial t} \tag{5}$$

where

$$g=-\frac{k(e)}{\gamma_w(1+e)}\left(\frac{\partial\sigma'}{\partial e}\right) \tag{6}$$

and

$$\lambda=-\frac{d}{de}\left(\frac{de}{d\sigma'}\right) \tag{7}$$

where $\lambda$ is denoted the linearization constant.

For application to the consolidation of soils, Gibson et al. [13] attempted to preserve the essential non-linearity of the permeability and compressibility by assuming that both $g$ and $\lambda$ are constants. However, concrete remains a frictional particulate material comparable to soil only until the degree of hydration reaches a threshold value at which a solid structure is formed [14]. As long as a water film separates the hydration products, fresh concrete has no intrinsic strength, but when the hydrated cement gel bridges the gaps between the hydrating cement particles, the development of the material strength and stiffness is initiated. The degree of hydration at which this occurs ranges from 6% to 30% [15,16], increasing with the water/cement ratio W/C [17].

To account for hydration in concrete, it is necessary to treat $g$ as a function of $t$. In the absence of suitable data to enable an appropriate function to be determined, it is assumed here that

$$g=g_0\left(1-\left(\frac{t}{t_s}\right)^m\right) \tag{8}$$

where $g_0$ is the finite-strain coefficient of consolidation at zero $t$, $t_s$ is the time at set, which is defined here as the point at which sufficient hydration has occurred to stop self-weight consolidation, and $m$ is a dimensionless exponent. In contrast, Tan et al. [7] and Josserand et al. [5] selected linear and exponential functions to account for the effects of hydration and set in their analyses.

Eq. (8) is plotted in Fig. 1 for $m$ values ranging from unity to infinity. Best-fit $m$ values ranging from 1.91 to 15.75 were obtained for the cement mortars and concretes analysed in the present study.

The parameter $g_0$ is given by

$$g_0=-\frac{k(e)}{\gamma_w(1+e)}\left(\frac{\partial\sigma'}{\partial e}\right) \tag{9}$$

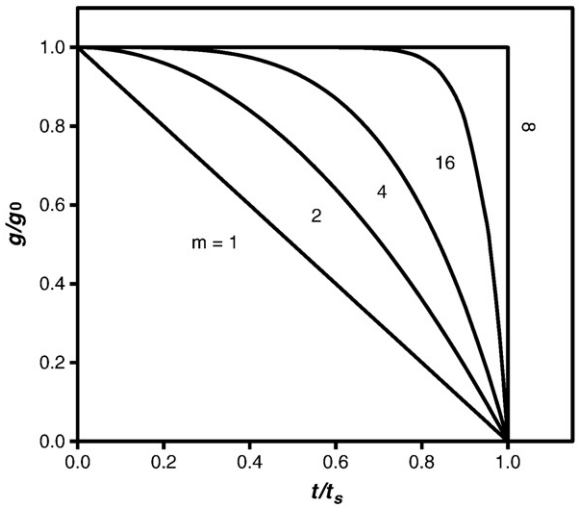


**Fig. 1.** Variation of finite-strain coefficient of consolidation with time.

where $k$, $e$, and $\sigma'$ refer to zero $t$. The assumption that $\lambda$ and $g_0$ are constant is valid only over limited ranges of $\sigma'$ and $e$ [18,19], and the same limitation applies to the analytical solutions based on Eqs. (3) and (5). However, this assumption has been shown to be satisfactory for soils, and hence is applicable to ordinary cement pastes, mortars, and concretes, which are much less variable materials. This will be confirmed by the results of the analyses of laboratory data presented subsequently.

The finite-strain $e$–$\sigma'$ relationship corresponding to constant $\lambda$, which can be obtained by integrating Eq. (7) and is thus implicit in Eq. (5), is [12,13]

$$e = (e_0 - e_\infty)\exp(-\lambda\sigma') + e_\infty \tag{10}$$

where $e_0$ is the $e$ corresponding to zero $\sigma'$ for finite-strain consolidation, and $e_\infty$ is the $e$ corresponding to infinite $\sigma'$.

Equating $\lambda$ to zero in Eq. (5) reduces it to the small-strain equation, Eq. (3). The corresponding linear $e$–$\sigma'$ relationship, which can be obtained by integrating Eq. (7) with $\lambda$ set to zero, is

$$e = e_0 - a_v\sigma' \tag{11}$$

where $a_v$ is the classical Terzaghi coefficient of compressibility [9].

The validity for concrete and similar materials of Eqs. (10) and (11), which were originally applied to soils, is demonstrated initially by Fig. 2 and ultimately by the subsequent validation of the equations for cumulative bleed derived using them. The representative finite-strain curve and small-strain line shown in Fig. 2 are based on consolidation test data for twenty-one specimens of retarded but otherwise ordinary Portland cement concrete [20]. The small-strain line is tangential to the finite-strain curve at zero $\sigma'$. The corresponding values of $e_0$, $e_\infty$, $\lambda$, and $a_v$ are 0.212, 0.182, 0.0163 $kPa^{-1}$, and $4.89\times10^{-4}$ $kPa^{-1}$, respectively. These are the means of the values derived by least-squares analyses of the consolidation data from all 21 tests. Very good fits were obtained in all cases, with the values of the correlation coefficient R and the F statistic ranging from 0.9949 to 0.9999 and from 56 to 6847, respectively. (The F statistic is the ratio of the variation in the data explained by the model to

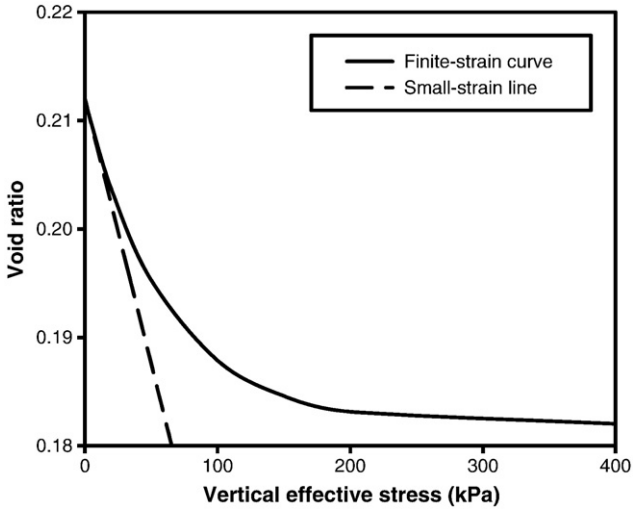


**Fig. 2.** Representative void ratio–effective stress relationships for finite- and small-strain consolidation.

the variation that remains unexplained. Hence an F value of 19 implies that the model fails to explain only 5% of the total variation in the data. Clearly, the higher the F value, the better the fit. Also, the F statistic enables the direct comparison of fits obtained for data sets of unequal sizes, while R does not.)

### 2.2. Normalised dimensionless governing equations

To obtain solutions of Eqs. (3) and (5), it is convenient to convert them into normalised dimensionless forms. This can be done by defining the parameters [13]

$$E(Z,T) = \frac{e(z,t)}{e(0,0)} \tag{12}$$

$$Z = \frac{z}{l} \tag{13}$$

$$T = \frac{g_0 t}{l^2} \tag{14}$$

and

$$N = \lambda l(\gamma_s - \gamma_w) \tag{15}$$

where $E$ is the normalised $e$, $Z$ is the dimensionless $z$, $T$ is the dimensionless time factor, $N$ is the dimensionless governing equation parameter, and $l$ is the depth of the concrete layer in material co-ordinates.

The substitution of Eqs. (12)–(15) in Eqs. (3) and (5), respectively, gives the normalised, dimensionless forms

$$\frac{\partial^2 E}{\partial Z^2}\left(1-\left(\frac{T}{T_s}\right)^m\right) = \frac{\partial E}{\partial T} \tag{16}$$

and

$$\left(\frac{\partial^2 E}{\partial Z^2} + N\frac{\partial E}{\partial Z}\right)\left(1-\left(\frac{T}{T_s}\right)^m\right) = \frac{\partial E}{\partial T} \tag{17}$$

Eq. (16) can obviously be obtained by equating $N$ to zero in Eq. (17). Eq. (15) shows that this implies either that $\lambda$ equals zero, the consequences of which have been discussed above; that $\gamma_c$ equals $\gamma_w$, i.e. that the buoyant weight of the solids in the concrete is zero; or that $l$ equals or closely approaches zero, i.e. the thickness of the concrete layer is small. The last two conditions both imply zero consolidation [12,19], and hence no bleeding.

### 2.3. Finite-strain analytical solutions for bleeding

The governing equation is Eq. (17). It is assumed that $e$ is initially constant over the whole depth of the concrete layer, which can drain freely at its upper surface but rests on impermeable material at its base. The initial, final, upper, and lower boundary conditions to be applied to Eq. (17) are, respectively.

$$E(Z,0) = 1; 0 \le Z \le 1 \tag{18}$$

$$\frac{\partial E(Z,T_s)}{\partial T} = 0; 0 \le Z \le 1 \tag{19}$$

$$E(0,T) = 1; 0 \le T \le T_s \tag{20}$$

and

$$\frac{\partial E(1,T)}{\partial Z} + N(E((1,T) - B) = 0; 0 \le T \le T_s \tag{21}$$

where $T_s$ is the dimensionless time factor at $t_s$, and $B$, the $E$ corresponding to infinite $\sigma'$, via Eq. (10), is given by

$$B = \frac{e_\infty}{e(0,0)} \tag{22}$$

Eq. (17) can be further simplified by transforming $T$ using the following relationship [21],

$$\partial\tau = \left(1-\left(\frac{T}{T_s}\right)^m\right)\partial T \tag{23}$$

where $\tau$ is the transformed dimensionless time factor.

Integrating Eq. (23) gives

$$\tau = T\left(1-\left(\frac{1}{m+1}\right)\left(\frac{T}{T_s}\right)^m\right) \tag{24}$$

Substituting Eq. (24) into Eqs. (17), (19), (20), and (21) gives

$$\frac{\partial^2 E}{\partial Z^2} + N\frac{\partial E}{\partial Z} = \frac{\partial E}{\partial \tau} \tag{25}$$

$$\frac{\partial E(Z,\tau_s)}{\partial T} = 0; 0 \le Z \le 1 \tag{26}$$

$$E(0,\tau) = 1; 0 \le \tau \le \tau_s \tag{27}$$

and

$$\frac{\partial E(1,\tau)}{\partial Z} + N(E((1,\tau)-B) = 0; 0 \le \tau \le \tau_s \tag{28}$$

where $\tau_s$ is the transformed dimensionless time factor at $t_s$.

The problem posed by the governing equation, Eq. (25), and the boundary conditions, Eqs. (18) and (26)–(28), has been solved previously for $\tau_s$ equal to infinity [12]. The existing solution for $E$, which remains valid if the upper limit for $\tau$ is reduced to $\tau_s$, is

$$E = (1-B)\exp(-NZ) + B + \exp\left(\frac{-NZ}{2}\right)\exp\left(\frac{-N^2\tau}{4}\right) \times \sum_{n=1}^{\infty}\left(D_n \sin(\alpha_n Z)\exp\left(-\alpha_n^2\tau\right)\right) \tag{29}$$

where $\alpha_n$ is the nth positive root of

$$\tan(\alpha) = \frac{-2\alpha}{N} \tag{30}$$

and

$$D_n = \frac{2(1-B)N\exp\left(\frac{N}{2}\right)\sin(\alpha_n)}{\alpha_n^2 + \left(\frac{N}{2}\right)^2 + \frac{N}{2}} \tag{31}$$

Substituting Eq. (24) in Eq. (29) gives the solution,

$$E = (1-B)\exp(-NZ) + B + \exp\left(\frac{-NZ}{2}\right)\exp\left(\frac{-N^2T}{4}\left(1-\left(\frac{1}{m+1}\right)\left(\frac{T}{T_s}\right)^m\right)\right) \times \sum_{n=1}^{\infty}\left(D_n \sin(\alpha_n Z)\exp\left(-\alpha_n^2 T\left(1-\left(\frac{1}{m+1}\right)\left(\frac{T}{T_s}\right)^m\right)\right)\right) \tag{32}$$

which is valid for $0 \le T \le T_s$, where $T_s \le \infty$.

In the absence of set, $T_s = \infty$, $\tau = T$, and Eq. (32) is reduced to the earlier solution for finite-strain self-weight consolidation [12].

The total depth of bleed at any time is obtained by subtracting the corresponding reduction in $E$ from the initial $E$ value of unity [Eq. (18)], and multiplying the result by the initial height of the pore water. This gives

$$b_t = le_i\left(1-\int_0^1 E(Z,T)dZ\right) \tag{33}$$

where $b_t$ is the total depth of bleed at time $t$.

Combining Eqs. (32) and (33) gives

$$b_t = le_i\left(1-\left(\frac{1-\exp(-N)}{N}\right)-\left(\begin{array}{l} 2N\exp\left(\frac{N}{2}\right)\exp\left(\frac{-N^2T}{4}\left(1-\left(\frac{1}{m+1}\right)\left(\frac{T}{T_s}\right)^m\right)\right) \\ \times \sum_{n=1}^{\infty}\left(\frac{\alpha_n \sin(\alpha_n)\exp\left(-\alpha_n^2 T\left(1-\left(\frac{1}{m+1}\right)\left(\frac{T}{T_s}\right)^m\right)\right)}{\left(\alpha_n^2 + \left(\frac{N}{2}\right)^2 + \frac{N}{2}\right)\left(\alpha_n^2 + \left(\frac{N}{2}\right)^2\right)}\right) \end{array}\right)\right) \tag{34}$$

which is valid for $0 \le T \le T_s$, where $T_s \le \infty$.

The solution for $b_t$ for the case where set does not occur before consolidation is complete can be obtained by equating $T_s$ to infinity in Eq. (34). This reduces it to

$$b_t = le_i\left(1-\left(\frac{1-\exp(-N)}{N}\right)-\left(\begin{array}{l}2N\exp\left(\frac{N}{2}\right)\exp\left(\frac{-N^2T}{4}\right)\\ \times\sum_{n=1}^{\infty}\left(\frac{\alpha_n\sin(\alpha_n)\exp\left(-\alpha_n^2T\right)}{\left(\alpha_n^2+\left(\frac{N}{2}\right)^2+\frac{N}{2}\right)\left(\alpha_n^2+\left(\frac{N}{2}\right)^2\right)}\right)\end{array}\right)\right) \tag{35}$$

which is valid for $0\le T\le\infty$.

### 2.4. Small-strain analytical solutions for bleeding

The problem is identical to that considered in Section 2.3, except that Eq. (16) is the governing equation, and the associated small-strain $e$–$\sigma'$ relationship, Eq. (11) (Fig. 2), applies.

The initial, final, and upper boundary conditions are given by Eqs. (18)–(20), respectively, and the lower boundary condition is given by

$$\frac{\partial E(1,T)}{\partial Z} = -A;\ 0\le T\le T_s \tag{36}$$

where $A$ is the slope of the $E$–$Z$ line, which is given by

$$A = \frac{(\gamma_s-\gamma_w)la_v}{e(0,0)} \tag{37}$$

Combining Eq. (16) and the boundary conditions with Eq. (23) again transforms the problem to one that has been solved previously for $\tau_s$ equal to infinity [12]. After $\tau_s$ is eliminated using Eq. (23), the existing solution for $E$, which again remains valid if the upper limit for $\tau$ is reduced to $\tau_s$, becomes

$$E = 1-AZ+\frac{8A}{\pi^2}\times\sum_{n=1,3,5}^{\infty}\left(\frac{1}{n^2}\sin\left(\frac{n\pi}{2}\right)\sin\left(\frac{n\pi Z}{2}\right)\exp\left(\frac{-n^2\pi^2T}{4}\left(1-\left(\frac{1}{m+1}\right)\left(\frac{T}{T_s}\right)^m\right)\right)\right) \tag{38}$$

Eq. (38) can also be obtained by equating $N$ and $NB$ to zero and $-A$, respectively, in Eqs. (30)–(32), the corresponding finite-strain solution [19]. The product $NB$ and $A$ remain finite in this case, because, although $N$ equals zero, $B$ [Eq. (22)] equals negative infinity (Fig. 2).

The total bleed is determined by substituting Eq. (38) in Eq. (33), giving

$$b_t = Ale_i\left(\frac{1}{2}-\frac{16}{\pi^3}\times\sum_{n=1,3,5}^{\infty}\left(\frac{1}{n^3}\sin\left(\frac{n\pi}{2}\right)\exp\left(\frac{-n^2\pi^2T}{4}\left(1-\left(\frac{1}{m+1}\right)\left(\frac{T}{T_s}\right)^m\right)\right)\right)\right) \tag{39}$$

which is valid for $0\le T\le T_s$, where $T_s\le\infty$.

The solution for $b_t$ for the case where set does not occur can be obtained by equating $T_s$ to infinity in Eq. (39). This gives

$$b_t = Ale_i\left(\frac{1}{2}-\frac{16}{\pi^3}\times\sum_{n=1,3,5}^{\infty}\left(\frac{1}{n^3}\sin\left(\frac{n\pi}{2}\right)\exp\left(\frac{-n^2\pi^2T}{4}\right)\right)\right) \tag{40}$$

which is valid for $0\le T\le\infty$.

## 3. Validation of analytical solutions

The finite- and small-strain analytical solutions for $b_t$, Eqs. (34), (35), (39) and (40), were validated by comparison with bleed test data for cement pastes [22] and concretes [23–25].

### 3.1. Comparison for cement pastes

Guo [22] conducted non-standard bleed tests in which ordinary Portland cement and water were combined at the W/C listed in Table 1. The initial height of the specimens was approximately 25 mm and the bleed was measured at 15 min intervals for the first 90 min and at 30 min intervals thereafter by weighing the specimens after the removal of all surface moisture. Evaporation of the bleed water thus had no effect on the results obtained. The total bleed ranged from 0.8 mm to 2.9 mm. A typical test result is shown in Fig. 3.

Eqs. (34), (35), (39) and (40) were fitted to the data using ordinary least-squares methods. The fitted finite- and small-strain curves were virtually indistinguishable in all cases (Fig. 3). The estimated $t_s$, the best-fitting equations, and the corresponding values of the fitting

**Table 1**
Best-fit analytical equations, fitting parameters, and statistics for bleeding of cement pastes.

| W/C | $t_s$ (min) | Best-fit equations | $m$ | $A$ | $N$ | $g_0$ (mm$^2$/s) | R | F |
|---|---|---|---|---|---|---|---|---|
| 0.35 | 120 | (34) | 3.40 | – | 0.524 | 0.0033 | 0.9994 | 2185 |
| | 120 | (39) | 3.35 | 0.504 | – | 0.0034 | 0.9994 | 2162 |
| 0.45 | 180 | (35) | – | – | 0.236 | 0.0196 | 0.9962 | 1048 |
| | 180 | (40) | – | 0.218 | – | 0.0214 | 0.9960 | 1005 |
| 0.55 | 180 | (35) | – | – | 0.417 | 0.0137 | 0.9990 | 3889 |
| | 180 | (40) | – | 0.365 | – | 0.0159 | 0.9988 | 3451 |

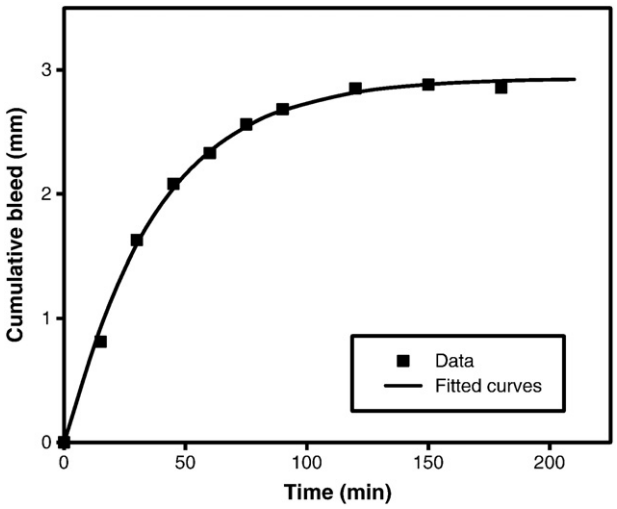


**Fig. 3.** Cumulative bleed versus time for cement paste with W/C of 0.55.

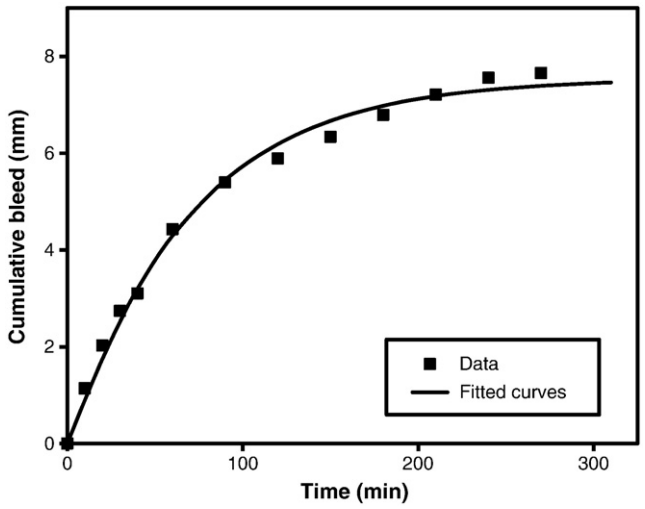


**Fig. 4.** Cumulative bleed versus time for mix A6.

parameters $m$, $A$, $N$, and $g_0$, and the R and F statistics obtained are listed in Table 1.

### 3.2. Comparison for concretes of Almusallam et al.

Almusallam et al. [23] conducted bleed tests in accordance with ASTM C 232 [26]. The bleed water was collected at 10 min intervals for the first 40 min and at 30 min intervals thereafter. The concrete specimens were made using Portland cement, crushed limestone coarse aggregate, and dune sand. The mix proportions are listed in Table 2. The slumps of the concrete mixes varied from 50 mm to 75 mm, and a high-range water reducer was used to obtain the desired workability. The initial height of the specimens was approximately 200 mm and the total bleed ranged from 0.2 mm to 8.0 mm. A typical test result is shown in Fig. 4. The least-squares fitting procedures used for the cement pastes were also used for the Almusallam et al. [23] bleed test data. The fitted finite- and small-strain curves were again virtually indistinguishable in all cases (Fig. 4). The results of the analyses are listed in Table 3.

### 3.3. Comparison for concretes of Zhan and Jia

Zhan and Jia [24] conducted bleed tests in accordance with AS 1012.6–1999 [27]. Ordinary Portland cement, fly ash, sand, gravel (Table 4), water reducer and retarder were used in all mixes, but shrinkage inhibitor was used in mixes Z2, Z4, and Z7 only. The desired slump of from 65 mm to 95 mm was obtained by adding water to the mix. Bleed water was collected at 10 min intervals for the first 30 min and at 30 min intervals thereafter. The initial height of the specimens was approximately 250 mm and the total bleed ranged from 0.4 mm to 1.4 mm. Typical test results are shown in Figs. 5 and 6. Repeat testing by Chan et al. [25] gave closely comparable results.

The same least-squares fitting procedures as before were used. However, because of initial reverse curvature in all of the cumulative bleed curves (Figs. 5 and 6) [24,25], it was necessary to use a false zero for the beginning of consolidation in order to fit the analytical solutions satisfactorily. The results of the analyses, including the values of the time shift d$t$ adopted to establish the false zero, are listed in Table 5. The fitted finite- and small-strain curves were again virtually indistinguishable (Figs. 5 and 6).

The cause of the initial reverse curvature of the cumulative bleed curves (Figs. 5 and 6) is uncertain, but it is probably attributable to a combination of initial elastic settlement [9], compression of entrained air [9], and an initial high rate of evaporation due to the initially low relative humidity of the air held in the containers used for the tests. The absence of similar reverse curvature in the cumulative bleed curves obtained by Almusallam et al. [23] for similar depths of concrete but often with considerably greater total depths of bleed (Fig. 4) suggests that the latter was the dominant effect. The d$t$ values listed in Table 5 can be accounted for completely by depths of evaporation ranging from 0.05 mm to 0.13 mm. Comparable results were obtained from the repeat tests [25].

**Table 2**
Concrete mix proportions used by Almusallam et al. [23].

| Mix | Cement ($kg/m^3$) | W/C | Cement:sand:gravel (by mass) |
|---|---|---|---|
| A1 | 300 | 0.40 | 1:2.2:4.4 |
| A2 | 300 | 0.50 | 1:2.1:4.2 |
| A3 | 300 | 0.65 | 1:2.0:4.0 |
| A4 | 350 | 0.40 | 1:1.8:3.6 |
| A5 | 350 | 0.50 | 1:1.7:3.2 |
| A6 | 350 | 0.65 | 1:1.6:3.2 |
| A7 | 400 | 0.40 | 1:1.5:3.0 |
| A8 | 400 | 0.50 | 1:1.4:2.8 |
| A9 | 400 | 0.65 | 1:1.3:2.6 |

**Table 3**
Best-fit analytical equations, fitting parameters, and statistics for bleed tests of Almusallam et al. [23].

| Mix | $t_s$ (min) | Best-fit equations | $m$ | $A$ | $N$ | $g_0$ ($mm^2/s$) | R | F |
|---|---|---|---|---|---|---|---|---|
| A1 | 40 | (34) | 1.93 | – | 0.562 | 0.39 | 0.9982 | 274 |
| | 40 | (39) | 1.93 | 0.535 | – | 0.41 | 0.9982 | 274 |
| A2 | 60 | (35) | – | – | 0.104 | 9.77 | 0.9983 | 1192 |
| | 60 | (40) | – | 0.101 | – | 10.13 | 0.9984 | 1226 |
| A3 | 210 | (35) | – | – | 0.194 | 4.29 | 0.9963 | 1222 |
| | 210 | (40) | – | 0.182 | – | 4.60 | 0.9962 | 1190 |
| A4 | 90 | (35) | – | – | 0.264 | 0.23 | 0.9547 | 51 |
| | 90 | (40) | – | 0.275 | – | 0.22 | 0.9547 | 51 |
| A5 | 180 | (35) | – | – | 0.174 | 3.53 | 0.9978 | 1798 |
| | 180 | (40) | – | 0.165 | – | 3.74 | 0.9978 | 1805 |
| A6 | 270 | (35) | – | – | 0.315 | 3.55 | 0.9961 | 1411 |
| | 270 | (40) | – | 0.285 | – | 3.96 | 0.9963 | 1491 |
| A7 | 120 | (35) | – | – | 0.079 | 7.97 | 0.9992 | 3933 |
| | 120 | (40) | – | 0.077 | – | 8.20 | 0.9993 | 4043 |
| A8 | 270 | (35) | – | – | 0.181 | 1.76 | 0.9965 | 1542 |
| | 270 | (40) | – | 0.172 | – | 1.87 | 0.9964 | 1533 |
| A9 | 270 | (35) | – | – | 0.302 | 2.73 | 0.9982 | 3071 |
| | 270 | (40) | – | 0.274 | – | 3.03 | 0.9984 | 3339 |

**Table 4**
Target strengths and concrete mix proportions used by Zhan and Jia [24].

| Mix | Target strength (MPa) | Cement ($kg/m^3$) | W/C | Cement:fly ash:sand:gravel (by mass) |
|---|---|---|---|---|
| Z1 and Z2 | 32 | 250 | 0.66 | 1:0.26:3.5:4.0 |
| Z3 and Z4 | 40 | 300 | 0.55 | 1:0.33:3.0:3.3 |
| Z5 | 40 | 305 | 0.54 | 1:0.33:2.4:3.9 |
| Z6 and Z7 | 50 | 380 | 0.43 | 1:0.32:1.6:2.7 |

In addition, initial setting times (i.e. the time elapsed since mixing) of 240 min and 370 min were determined for mixes Z1 and Z6, respectively [25], by penetration resistance in accordance with AS 1012.18–1996 [28] (Fig. 7). The initial set conventionally corresponds to a penetration resistance of 3.5 MPa.

### 3.4. Discussion of results of comparisons

Tables 1, 3, and 5 show that very high R and F values and hence very good fits were obtained in all cases for both the finite- and small-strain solutions. Eqs. (34) and (39), which account for hydration and set, gave the best fits in fourteen of the twenty-six cases analysed, while Eqs. (35) and (40), which do not, gave the best fits in the remainder. This is consistent with the views of Powers [1], Tan et al. [6], Tan et al. [7], and Josserand et al. [5] that theoretical models of bleeding must be able to account for set.

The fits obtained also justify the neglect in the present solutions of the effect on bleeding of temperature changes, including those caused by the heat of hydration [4]. This outcome is unsurprising, because the primary effect of increasing temperature is to reduce the viscosity of the water in the pores in the concrete and hence increase both its permeability and the bleed rate. Over the normal temperature range for fresh cement pastes, cement mortars, and concretes, however, the effect is comparatively small. Almost all other models of bleeding also neglect the effect of temperature changes [1,5–7].

Furthermore, there was very little to choose between the small- and finite-strain solutions in all cases; as noted above they are virtually indistinguishable (Figs. 3–6). This appears to contradict the assertion of Josserand et al. [5] that theoretical models of bleeding must be able to accommodate relatively large strains. However, concrete with maximum depths of only about 250 mm was analysed. The corresponding maximum $\sigma'$ is about 4.2 kPa, well within the range of effective stress where the finite-strain curve and the small-strain lines for concrete shown in Fig. 2 are essentially indistinguishable. Although Fig. 2 represents only a single group of test results, this suggests strongly that the very similar results obtained for the finite- and small-strain solutions were only to be expected.

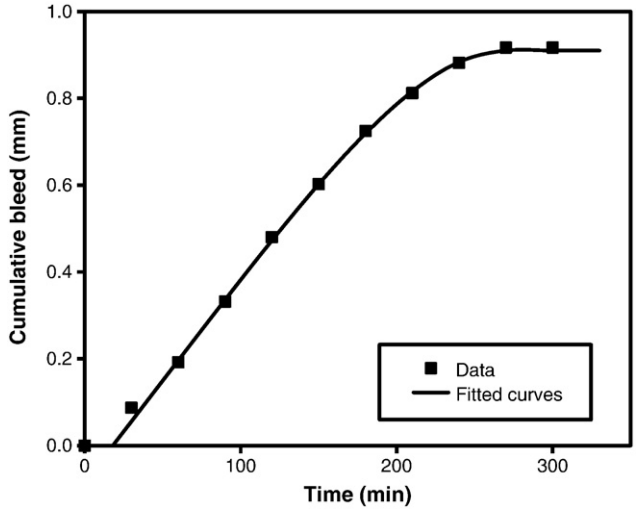


**Fig. 5.** Cumulative bleed versus time for mix Z1, specimen 1.

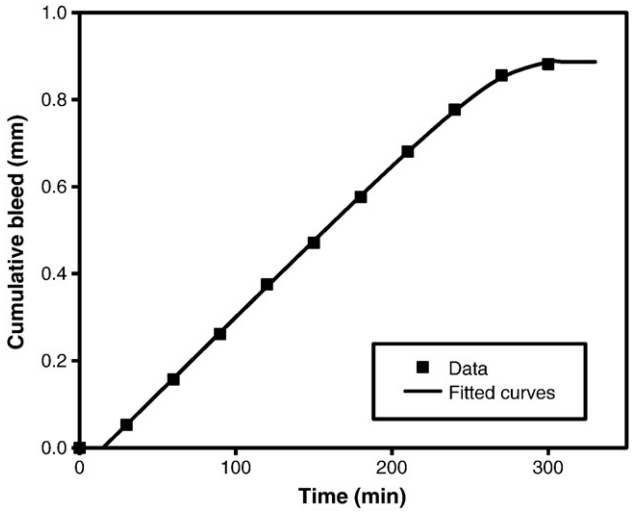


**Fig. 6.** Cumulative bleed versus time for mix Z7, specimen 1.

Moreover, cement pastes [6,7,22], cement mortars [7], and concretes [23–25] are all characterised by relatively low initial void ratios. This alone might be sufficient to ensure that small-stain solutions are adequate to describe the bleeding of comparatively deep sections. Further research is required to verify this.

## 4. Application of analytical solutions to prediction

The input data required to predict bleed rates and total bleed using the small-strain solution comprise values of $l$, $e_i$, $t_s$, $g_0$, $m$, and $A$. The input data required for the finite-strain solution are identical except that $N$ replaces $A$. Both $l$ and $e_i$ can be readily determined in any given case and need not be considered further here.

The need to evaluate $t_s$ has been noted by Josserand et al. [5]. The times of initial set for mixes Z1 and Z6 (approximately 240 min and 270 min, respectively) determined by penetration resistance tests (Fig. 7) are roughly comparable to the corresponding $t_s$ values (270 min and 240 min) determined by bleed tests (Table 5 and Fig. 5). The initial set times and $t_s$ are measured from different starting points, namely from the addition of water to the mix and from the end of placement, respectively, but, for the experiments described, the difference, although not known precisely, was relatively small. This suggests that, with appropriate adjustment for the delay between the addition of mix water and the end of placement, the time of initial set could be used to estimate $t_s$ for the application of the new analytical solutions to the prediction of the bleeding of full-scale concrete pours.

To enable the application of the new solutions to the prediction of bleeding, it will also be necessary to determine predictive relationships for $g_0$, $m$, $A$, and $N$ based on mix parameters such as the W/C and $e_i$ [5]. The results of the analyses presented in Tables 1, 3, and 5, and Eq. (8) (Fig. 1) suggest strongly that to evaluate $g_0$, $m$, $A$, and $N$, it is necessary to model the kinetics of hydration, which are material specific. For any given mix, the four parameters are most readily evaluated by conducting a bleed test and fitting the new solutions to the resulting data. Alternatively, they can be evaluated with significantly greater effort but independently of the new solutions from the results of a series of five or six fast oedometer (consolidation) tests with staggered starting times and hence different initial degrees of hydration [7]. The required predictive relationships can be based on the results of both types of test [5,7] for representative ranges of cement pastes, cement mortars, and concretes. This is the subject of ongoing research.

**Table 5**
Best-fit analytical equations, fitting parameters, and statistics for bleed tests of Zhan and Jia [24].

| Mix. specimen | $t_s$ (min) | Best-fit equations | d$t$ (min) | $m$ | $A$ | $N$ | $g_0$ (mm$^2$/s) | R | F |
|---|---|---|---|---|---|---|---|---|---|
| Z1.1 | 270 | (34) | 18 | 4.38 | – | 0.136 | 0.576 | 0.9998 | 7080 |
| | 270 | (39) | 18 | 4.34 | 0.134 | – | 0.583 | 0.9998 | 7049 |
| Z1.2 | 270 | (34) | 23 | 2.96 | – | 0.151 | 0.565 | 0.9990 | 1281 |
| | 270 | (39) | 23 | 2.95 | 0.149 | – | 0.572 | 0.9990 | 1277 |
| Z2.1 | 270 | (35) | 21 | – | – | 0.121 | 0.871 | 0.9988 | 2555 |
| | 270 | (40) | 21 | – | 0.117 | – | 0.898 | 0.9988 | 2501 |
| Z2.2 | 270 | (35) | 15 | – | – | 0.186 | 0.535 | 0.9962 | 794 |
| | 270 | (40) | 15 | – | 0.180 | – | 0.554 | 0.9962 | 787 |
| Z3.1 | 240 | (34) | 30 | 15.55 | – | 0.643 | 0.075 | 0.9987 | 749 |
| | 240 | (39) | 30 | 15.55 | 0.767 | – | 0.063 | 0.9987 | 749 |
| Z3.2 | 240 | (34) | 17 | 16.82 | – | 0.595 | 0.089 | 0.9987 | 776 |
| | 240 | (39) | 17 | 16.83 | 0.869 | – | 0.061 | 0.9987 | 776 |
| Z4.1 | 300 | (34) | 25 | 10.59 | – | 0.545 | 0.100 | 0.9997 | 5621 |
| | 300 | (39) | 25 | 10.59 | 0.635 | – | 0.102 | 0.9997 | 5621 |
| Z4.2 | 300 | (34) | 28 | 12.17 | – | 0.635 | 0.102 | 0.9999 | 11,281 |
| | 300 | (39) | 28 | 12.13 | 0.154 | – | 0.416 | 0.9999 | 11,337 |
| Z5.1 | 270 | (34) | 37 | 5.54 | – | 0.089 | 0.414 | 0.9990 | 1260 |
| | 270 | (39) | 37 | 5.52 | 0.089 | – | 0.415 | 0.9990 | 1260 |
| Z5.2 | 270 | (34) | 33 | 5.11 | – | 0.125 | 0.299 | 0.9979 | 585 |
| | 270 | (39) | 33 | 5.10 | 0.125 | – | 0.300 | 0.9979 | 585 |
| Z6.1 | 240 | (34) | 28 | 4.86 | – | 0.150 | 0.307 | 0.9987 | 792 |
| | 240 | (39) | 28 | 4.85 | 0.149 | – | 0.309 | 0.9987 | 792 |
| Z6.2 | 240 | (34) | 27 | 3.05 | – | 0.087 | 0.581 | 0.9990 | 957 |
| | 240 | (39) | 27 | 3.04 | 0.086 | – | 0.585 | 0.9990 | 955 |
| Z7.1 | 300 | (34) | 15 | 7.58 | – | 0.519 | 0.114 | 0.9999 | 16,693 |
| | 300 | (39) | 15 | 7.58 | 0.537 | – | 0.110 | 0.9999 | 16,692 |
| Z7.2 | 300 | (34) | 22 | 6.71 | – | 0.650 | 0.094 | 0.9999 | 35,613 |
| | 300 | (39) | 22 | 6.72 | 0.493 | – | 0.124 | 0.9999 | 35,587 |

## 5. Summary and conclusions

New analytical finite- and small-strain solutions for the bleeding of cement pastes, cement mortars, and concrete modelled as self-weight consolidation have been presented that account for the effects of hydration and set. The solutions have been validated by comparison with laboratory data for cement pastes and concretes taken from three different sources. They are more comprehensive than the earlier analytical solution of Tan et al. [6] and numerical solution of Kwak and Ha [4], which are restricted to small stains and ignore the effects of hydration, and are simpler to implement than the comparable numerical solutions of Tan et al. [7] and Josserand et al. [5].

It has been shown that the finite- and small-strain solutions represent the data equally well, and hence that the small-strain model was adequate to represent all of the cases investigated. This is consistent with the relatively shallow depths of the specimens analysed, but is also consistent with the relatively low initial void ratios characteristic of cement pastes, cement mortars, and concretes. Further research is required to establish whether the small-strain solutions can model adequately the bleeding of comparatively thick concrete.

To enable the new analytical solutions to be applied to the prediction of bleeding in both small and large structures, it will also be necessary to develop quick tests or correlations for several mix- and pour-specific parameters that are required as input data. As a first step towards this, it has been shown here that it might be possible to use the time of initial set obtained from a standard small-scale penetration resistance test to estimate the time of set and hence the end of consolidation bleeding in a full-scale concrete pour. However, further research is required to confirm this.

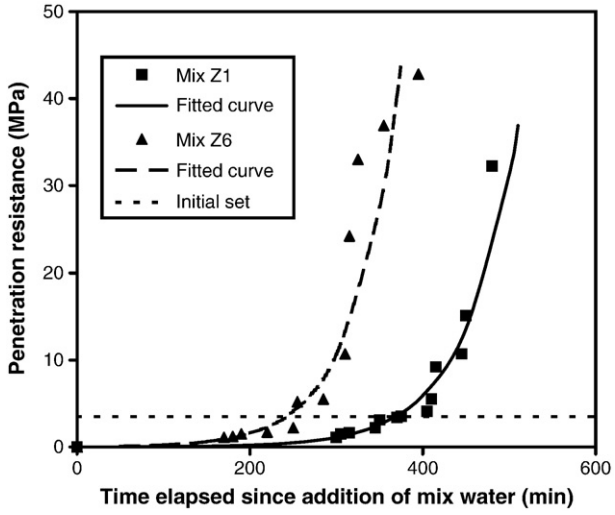


**Fig. 7.** Variation with time of penetration resistances of mixes Z1 and Z2.

*Nomenclature*

*Greek*

| | |
|---|---|
| $\alpha_n$ | nth positive root of Eq. (30) |
| $\gamma_s$ | unit weight of solids (N/m$^3$) |
| $\gamma_w$ | unit weight of water (N/m$^3$) |
| $\lambda$ | linearization constant (Pa$^{-1}$) |
| $\sigma'$ | vertical effective stress (Pa) |
| $\tau$ | transformed dimensionless time factor |
| $\tau_s$ | transformed dimensionless time factor at set |

*Latin*

| | |
|---|---|
| W/C | water/cement ratio |
| $a_v$ | Terzaghi coefficient of compressibility (Pa$^{-1}$) |
| $A$ | slope of normalised void ratio–dimensionless vertical material co-ordinate line |
| $b_t$ | total depth of bleed at time $t$ (m) |
| $B$ | normalised void ratio at infinite vertical effective stress |
| $c_v$ | Terzaghi small-strain coefficient of consolidation (m$^2$/s) |
| $D_n$ | nth coefficient in Eq. (29) |

| | |
|---|---|
| $dt$ | time shift to establish false zero for consolidation model (s) |
| $e$ | void ratio |
| $e_i$ | void ratio at zero time |
| $e_0$ | void ratio at zero vertical effective stress |
| $e_\infty$ | void ratio at infinite vertical effective stress |
| $E$ | normalised void ratio |
| $g$ | finite-strain coefficient of consolidation ($m^2/s$) |
| $g_0$ | finite-strain coefficient of consolidation at zero time ($m^2/s$) |
| $k$ | vertical permeability (m/s) |
| $l$ | depth of concrete layer in material co-ordinates (m) |
| $m$ | dimensionless exponent in Eq. (8) |
| $N$ | dimensionless governing equation parameter |
| $t$ | time (s) |
| $t_s$ | time at set (s) |
| $T$ | dimensionless time factor |
| $T_s$ | dimensionless time factor at set |
| $x$ | vertical natural co-ordinate measured downwards from top of concrete (m) |
| $z$ | vertical material co-ordinate measured downwards from top of concrete (m) |
| $Z$ | dimensionless vertical material co-ordinate |

## Acknowledgment

The research was funded by the Queensland Department of Main Roads.

## References

[1] T.C. Powers, The Bleeding of Portland Cement Paste, Mortar and Concrete Treated as a Special Case of Sedimentation, Research Laboratory of the Portland Cement Association, Chicago, 1939.
[2] J.C. Sprague, Evaluating fines on a bleeding test basis, J. Am. Conc. Inst. 33 (5) (1936) 29–40.
[3] P.H. Morris, P.F. Dux, A review of the ACI recommendations for the prevention of plastic cracking, Am. Conc. Inst. Mat. J. 102 (5) (2005) 307–314.
[4] H.G. Kwak, S.J. Ha, Plastic shrinkage cracking of concrete slabs. Part I, a numerical model, Mag. Conc. Res. 58 (8) (2006) 505–516.
[5] L. Josserand, O. Coussey, F. de Larrard, Bleeding of concrete as an ageing consolidation process, Cem. Conc. Res. 36 (9) (2006) 1603–1608.
[6] T.S. Tan, T.H. Wee, S.A. Tan, C.T. Tam, S.L. Lee, A consolidation model for bleeding of cement paste, Adv. Cem. Res. 1 (1) (1987) 18–26.
[7] T.S. Tan, C.K. Loh, K.Y. Yong, T.H. Wee, Modelling the bleeding of cement paste and mortar, Adv. Cem. Res. 9 (34) (1997) 75–91.
[8] K. Lee, G.C. Sills, The consolidation of a soil stratum, including self-weight effects and large strains, Int. J. Num. Analyt. Meth. Geomech. 5 (4) (1981) 405–428.
[9] K. Terzaghi, Theoretical Soil Mechanics, Chapman and Hall, London, 1943.
[10] R.E. Gibson, G.L. England, M.J.L. Hussey, The theory of one-dimensional consolidation of clays, Geotechnique 17 (3) (1967) 261–273.
[11] A. McNabb, A mathematical treatment of one-dimensional soil consolidation, Quart. Appl. Math. 17 (4) (1960) 337–347.
[12] P.H. Morris, Analytical solutions of linear-finite strain one-dimensional consolidation, Am. Soc. Civ. Engrs. J. Geotech. Geoenvir. Engng. 128 (4) (2002) 319–326.
[13] R.E. Gibson, R.L. Schiffman, K.W. Cargill, The theory of one-dimensional consolidation of saturated clays. II. Finite nonlinear consolidation of thick homogeneous layers, Can. Geotech. J. 18 (2) (1981) 280–293.
[14] D. Gawin, F. Pesavento, B.A. Schreffer, Hygro-thermo-chemo-mechanical modelling of concrete at early ages and beyond. Part I, hydration and hygro-thermal phenomena, Int. J. Num. Meth. Engng. 67 (3) (2006) 299–331.
[15] G. De Schutter, L. Taerwe, Degree of hydration-based description of mechanical properties of early age concrete, Mat. Struct. 29 (190) (1996) 335–344.
[16] F.J. Ulm, O. Coussey, Strength growth as chemo-plastic hardening in early age concrete, Am. Soc. Civ. Engrs. J. Engng. Mechs. 122 (12) (1996) 1123–1132.
[17] G. De Schutter, Influence of hydration reaction on engineering properties of hardening concrete, Mat. Struct. 35 (252) (2002) 447–452.
[18] D. Znidarcic, R.L. Schiffman, V. Pane, P. Croce, H.Y. Ho, H.W. Olsen, The theory of one-dimensional consolidation of saturated clays: part V. Constant rate of deformation testing and analysis, Geotechnique 36 (2) (1986) 227–237.
[19] P.H. Morris, Analytical solutions of finite- and small-strain one-dimensional consolidation, Int. J. Num. Analyt. Meth. Geomech. 29 (2) (2005) 127–140.
[20] O.J. Uzomaka, Some fundamental engineering properties of plastic concrete, PhD thesis, University of Newcastle upon Tyne, 1969.
[21] J. Crank, The Mathematics of Diffusion, Clarendon Press, Oxford, 1956.
[22] C. Guo, Early-age behaviour of Portland cement paste, Am. Conc. Inst. Mat. J. 91 (1) (1994) 13–25.
[23] A.A. Almusallam, M. Maslehuddin, M. Abdul-Waris, M.M. Kahn, Effect of mix proportions on plastic shrinkage cracking of concrete in hot environments, Const. Build. Mat. 12 (6–7) (1998) 353–358.
[24] N.T. Zhan, Q. Jia, The Influence of Chemical Constituents on the Bleeding of Concrete, MEng Research Project Report, University of Queensland, 2005.
[25] T.C. Chan, C.Y. Phua, P.C. Tan, Bleeding of concrete. BE thesis project report, University of Queensland, 2007.
[26] American Society for Testing and Materials, ASTM C 232-04 Standard Test Methods for Bleeding of Concrete, American Society for Testing and Materials, West Conshohoken, PA, 2004.
[27] Standards Australia, AS 1012.6–1999, Method for the Determination of Bleeding of Concrete, Standards Australia, Sydney, 1999.
[28] Standards Australia, AS 1012.18–1996, Determination of Setting Time of Fresh Concrete, Mortar and Grout by Penetration Resistance, Standards Australia, Sydney, 1996.